

Finite Element Modeling of Viscoelastic Behavior and Interface Damage in Adhesively Bonded Joints

Feifei Cheng, Ö. Özgü Özsoy and J.N. Reddy*

*Advanced Computational Mechanics Laboratory, Department of Mechanical Engineering,
Texas A&M University, College Station, TX, 77843-3123, USA*

Abstract

This paper presents a study on viscoelastic behavior of the adhesive and damage analysis of adhesive-adherend interfaces in adhesively bonded joints. First, viscoelastic finite element analysis of a model joint with viscoelastic adhesive has been conducted while considering geometric nonlinearity as well as thermal expansion. Then a finite element model for bond failure analysis at the viscoelastic adhesive-elastic adherend interface for a mixed-mode fracture problem is proposed. In the framework of cohesive zone model, traction-separation law is used to define the constitutive response of the cohesive elements at the interface. Quadratic nominal stress criterion and mixed-mode energy criterion are used to determine the damage initiation and evolution at the interface, respectively.

Keywords: adhesive joints, finite element, viscoelasticity, damage, cohesive elements

1. Introduction

Advances in polymer technologies have increased the use of the polymeric adhesives to join dissimilar material structural components together. Adhesively bonded joints are widely used in aerospace and automotive industries as well as in various other structural systems. They are considered to be more efficient compared to the conventional fasteners such as bolts, rivets, and welded joints, which cause high stress concentrations. Bonded joints are of great importance due to the advantages in terms of their light weight compared to the mechanical fastening and efficiency of joining, good damping and fatigue characteristics.

The lap shear test is the most widely used method for producing in-situ shear strength data on adhesively bonded joints. Some of the characteristics of a lap joint are as follows: tensile stress is exerted over the entire joint and away from the adhesive bond; shear stress is exerted across the adhesive bond (i.e., the bonded materials are forced to slide over each other); cleavage stress is concentrated at one edge and exerts a prying force on the bond; and peel stress is concentrated along a thin line at the bond's edge. However, the stresses generated in the adhesive layer are not uniform. The eccentricity of the axis of a lap joint gives rise to transverse or peel stresses at the

*Corresponding author.

E-mail address: jnreddy@tamu.edu (J.N. Reddy)

Report Documentation Page

Form Approved
OMB No. 0704-0188

Public reporting burden for the collection of information is estimated to average 1 hour per response, including the time for reviewing instructions, searching existing data sources, gathering and maintaining the data needed, and completing and reviewing the collection of information. Send comments regarding this burden estimate or any other aspect of this collection of information, including suggestions for reducing this burden, to Washington Headquarters Services, Directorate for Information Operations and Reports, 1215 Jefferson Davis Highway, Suite 1204, Arlington VA 22202-4302. Respondents should be aware that notwithstanding any other provision of law, no person shall be subject to a penalty for failing to comply with a collection of information if it does not display a currently valid OMB control number.

| | | | |
|--|------------------------------------|---|---|
| 1. REPORT DATE 2012 | 2. REPORT TYPE | 3. DATES COVERED 00-00-2012 to 00-00-2012 | |
| 4. TITLE AND SUBTITLE Finite Element Modeling of Viscoelastic Behavior and Interface Damage in Adhesively Bonded Joints | | 5a. CONTRACT NUMBER | |
| | | 5b. GRANT NUMBER | |
| | | 5c. PROGRAM ELEMENT NUMBER | |
| 6. AUTHOR(S) | | 5d. PROJECT NUMBER | |
| | | 5e. TASK NUMBER | |
| | | 5f. WORK UNIT NUMBER | |
| 7. PERFORMING ORGANIZATION NAME(S) AND ADDRESS(ES) Texas A&M University, Department of Mechanical Engineering, Advanced Computational Mechanics Laboratory, College Station, TX, 77843 | | 8. PERFORMING ORGANIZATION REPORT NUMBER | |
| 9. SPONSORING/MONITORING AGENCY NAME(S) AND ADDRESS(ES) | | 10. SPONSOR/MONITOR'S ACRONYM(S) | |
| | | 11. SPONSOR/MONITOR'S REPORT NUMBER(S) | |
| 12. DISTRIBUTION/AVAILABILITY STATEMENT Approved for public release; distribution unlimited | | | |
| 13. SUPPLEMENTARY NOTES Special Issue of Journal of Adhesion Science and Technology, 2012 (in press) | | | |
| 14. ABSTRACT This paper presents a study on viscoelastic behavior of the adhesive and damage analysis of adhesive-adherend interfaces in adhesively bonded joints. First, viscoelastic finite element analysis of a model joint with viscoelastic adhesive has been conducted while considering geometric nonlinearity as well as thermal expansion. Then a finite element model for bond failure analysis at the viscoelastic adhesive-elastic adherend interface for a mixed-mode fracture problem is proposed. In the framework of cohesive zone model, traction-separation law is used to define the constitutive response of the cohesive elements at the interface. Quadratic nominal stress criterion and mixed-mode energy criterion are used to determine the damage initiation and evolution at the interface, respectively. | | | |
| 15. SUBJECT TERMS | | | |
| 16. SECURITY CLASSIFICATION OF: | | | 17. LIMITATION OF ABSTRACT Same as Report (SAR) |
| a. REPORT unclassified | b. ABSTRACT unclassified | c. THIS PAGE unclassified | |
| 19a. NAME OF RESPONSIBLE PERSON | | | |

ends of the overlap, enabling cracks to initiate and propagate from the ends of the overlap. The present study is concerned with stress distribution and crack propagation in elastic and viscoelastic adhesive joints. The following literature review, by no means exhaustive or complete, provides a background for the present study.

Adams and Peppiatt [1] focused on the stresses at the end of the adhesive layer of adhesively bonded lap joints. They formulated a plane-strain problem, in which the shear deformations and bending of the adherends are taken into account. They also showed the effect of the adhesive thickness on the strength of the joint. Ojalvo and Eidinoff [2] also discussed the adhesive thickness effects upon stresses in single lap joints (SLJs) by extending the analytical approach of Goland and Reissner [3], through the use of a more complete shear strain-displacement equation for the adhesive layer. Delale et al. [4] solved the SLJ as a plane strain problem in which the adherends are considered as orthotropic plates for which a transverse shear deformation theory is used. Their solution does not provide zero stress condition at the free ends of the adhesive layer. Zhao et al. [5, 6] developed a model capable of providing an explicit closed-form solution for the elastic stress analysis in SLJs. The theory can predict zero shear stress condition at the free ends of the adhesive, as well as the variation of the normal stress through the adhesive thickness.

Reddy and Roy [7] used the updated Lagrangian formulation for elastic solids to develop a two-dimensional finite element analysis with geometric nonlinearity. They brought attention to the effect of boundary conditions applied at the ends of the adherends and mesh on the stress distributions in lap joints. Carpenter [8] formulated a finite element analysis approach in which finite thickness of adhesive is accounted for. It is based on the assumptions common to the theories of Goland and Reissner [3], and Ojalvo and Eidinoff [2]. He developed two different elements based on the formulation of aforementioned theories. Cooper and Sawyer [9] derived the Goland and Reissner equations for adhesive shear and peel stresses. The development of the equations is similar to the original with some slight modifications to improve the consistency of the analysis. Li et al. [10] used nonlinear finite element analysis to investigate the stress and strain distributions across the adhesive thickness in SLJs where the adherends consist of composite material. They also proposed a methodology to treat the cohesive failure in the adhesive layer and possible failure mechanisms. Magalhães et al. [11] investigated the stress distributions along the overlap at various cross sections of the SLJs and concluded that the highest stresses are found at the top and bottom interfaces, at the end of the overlap region. This indicates that damage can initiate at these interfaces. Yang et al. [12] developed an elastoplastic analytical model for SLJs. They assumed that the adherends are linear elastic, whereas the adhesives are elastic-perfectly

plastic following the von Mises yield criterion. It is claimed that the model developed in this study is a good tool to evaluate the joint strength under the cohesive failure model once a suitable joint failure criterion is established.

The finite element method has also been used by several researchers to model viscoelastic behavior of adhesively bonded joints: Yadagiri et al. [13] employed usual and modified plane strain systems in formulating the adhesive layer element. Carpenter [14] used direct integration process to advance the solution with time. Henriksen [15] used nonlinear viscoelastic model proposed by Schapery [16] and compared the numerical results with the experimental results of Peretz and Weitsman [17]. Knauss and Emri's nonlinear viscoelastic model [18] has been employed by Becker et al. [19] in developing a finite element program named VISTA for stress analysis of adhesively bonded joints. In Roy and Reddy's work [20-22], an updated Lagrangian formulation and the associated Schapery's nonlinear viscoelastic finite element model were developed; the nonlinear viscoelastic behavior has been studied and compared with the results from VISTA by Becker et al.'s work [19]; they also studied the effect of moisture on stress distributions in adhesive joints. Schapery's viscoelastic model combined with elastoplastic constitutive relation was used to carry out finite element analysis of unidirectional composite laminate by Schaffer and Adams [23].

Experimental and theoretical studies of crack propagation in a viscoelastic medium have been carried out by a number of authors [24-29]. Finite element analysis of crack propagation in bonded joints in which adhesives have viscoelastic properties has been conducted in [30-34]. In Allen and Searcy's work [30], a micromechanical model for a viscoelastic cohesive zone was formulated while traction-displacement law has been integrated numerically in an implicit finite element formulation to predict crack propagation in double cantilever beam (DCB) model. Chen and Dillard [31] conducted numerical analysis of the directionally unstable crack propagation in adhesively bonded joints by using interface mechanics and the finite element method. Dubois et al. [32] studied the effects of viscoelastic characteristics on the creep-crack growth process, in which fracture parameters are computed through a coupling process with an incremental viscoelastic formulation. Rahul Kumar and coworkers [33] used cohesive elements for the region ahead of the crack tip in modeling of fracture propagation in peel test on viscoelastic material. Their dimensional analysis showed that the macroscopic fracture energy scales with the intrinsic fracture toughness and is a function of peel velocity, and parameters such as the thickness, bulk properties of the polymer sheets, and other cohesive zone properties. Muliana and Khan [34] developed a time-integration algorithm for thermo-rheological complex material (TCM), and

conducted finite element analysis of crack propagation in adhesively bonded joint systems with TCM type polymer adhesives for fracture Mode I and Mode II. In their model, a crack path was predetermined at the mid-height of the adhesive layers, where one layer of cohesive elements is applied along.

It should be noted that most of the above studies regarding finite element analysis of crack propagation in bonded joints with viscoelastic adhesive are developed for those cases in which crack lies within the adhesive and mostly for peel testing (fracture Mode I). In this paper, a cohesive-zone based finite element model has been constructed to study the bond failure behavior at the viscoelastic adhesive-elastic adherend interface for a mixed-mode fracture problem (Mode I and Model II).

2. Finite element analysis of viscoelastic adhesively bonded joints

2.1. Constitutive relation

In the integral form of linear viscoelasticity, the stress is expressed in terms of the strain history as

$$\mathbf{S}(t) = \int_{-\infty}^t G(t-s)\dot{\boldsymbol{\varepsilon}}(s)ds, \quad \text{where } \boldsymbol{\varepsilon} = \nabla u + \nabla u^T, \quad \dot{\boldsymbol{\varepsilon}} = \nabla v + \nabla v^T, \quad \mathbf{S} = \boldsymbol{\sigma} + p\mathbf{I} \quad (1)$$

where \mathbf{S} is the deviatoric stress tensor, t is the current time, G is the time-dependent shear relaxation modulus, $\boldsymbol{\varepsilon}$ is the engineering strain tensor, $\boldsymbol{\sigma}$ is the total stress tensor, p is the hydrostatic pressure, and \mathbf{I} is the unit tensor.

For linear viscoelastic model, Prony series expansion of the dimensionless relaxation modulus $g_R(t)$ can be expressed as follows,

$$g_R(t) = 1 - \sum_{i=1}^N g_i (1 - e^{-t/\tau_i}) \quad (2)$$

where N, g_i, τ_i are material constants. For adhesive material FM-73 (Chemical type: elastomer epoxy; Manufacture: American Cyanamid) used in this study, compliance modulus $D(t)$ is given in [21] as:

$$D(t) = 0.5988 \times 10^{-3} + 1.637 \times 10^{-5} (1 - e^{-t/0.01}) + 0.6031 \times 10^{-4} (1 - e^{-t/0.1}) \\ + 0.9108 \times 10^{-4} (1 - e^{-t/1.0}) + 2.6177 \times 10^{-4} (1 - e^{-t/10.0}) \quad (3)$$

Since for viscoelastic analysis, stress formulation equation (1) is used in the present analysis, we will have to transform creep compliance $D(t)$ to relaxation modulus $E(t)$ and obtain the corresponding Prony series expression. From the linear theory of viscoelasticity, the relation between relaxation modulus and creep compliance can be derived in the following way (see Reddy [35], p. 312):

Given $\sigma(t) = \sigma_0 H(t) = 1 \cdot H(t)$, then we have

$$1 = D(0)E(t) + \int_0^t E(t-s) \frac{dD(s)}{ds} ds, \quad \frac{1}{s^2} = \bar{E}(s)\bar{D}(s) \quad (4)$$

Using inverse Laplace Transformation to calculate $E(t)$ from $D(t)$, we can obtain the dimensionless relaxation modulus

$$\begin{aligned} g_R(t) &= 1 - \sum_{i=1}^N g_i \left(1 - e^{-t/\tau_i}\right) \\ &= 1 - 0.02728 \times \left(1 - e^{-t/0.009731}\right) - 0.08933 \times \left(1 - e^{-t/0.090992}\right) \\ &\quad - 0.1098 \times \left(1 - e^{-t/0.878503}\right) - 0.1912 \times \left(1 - e^{-t/7.491198}\right) \end{aligned} \quad (5)$$

In [36], the Prony series parameters g_i and τ_i can be defined directly from each term in equation (5).

2.2. Numerical example

The model joint analysis problem presented in [21] is used as the validation example. The geometry, boundary conditions and loading are shown in Figure 1. It has a total length of 132.1 mm, with thickness 12.91 mm, and overlap length 12.7 mm. The adhesive thickness is 0.254 mm. On the left hand side of the model joint, horizontal and vertical displacements $u_x = u_y = 0$ are applied; while on the right hand side, vertical displacement $u_y = 0$ is applied at top and bottom corners of adherend. Uniform stress $q_x = 13.6$ MPa is applied at the right end. The material properties of Al adherend, adhesive FM-73 are listed in Table 1.

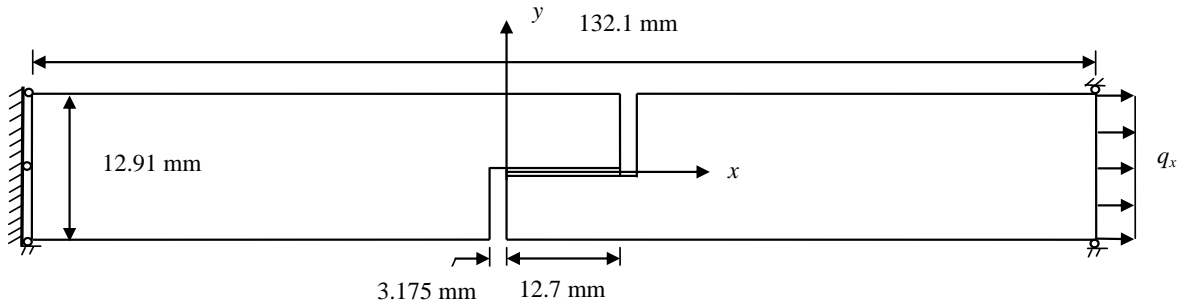


Figure 1: Geometry, boundary conditions and loading for the model joint.

Table 1. Material properties of Al and FM-73 [21].

| Material | Young's Modulus E (GPa) | Poisson's Ratio ν | CTE α ($10^{-6}/^{\circ}\text{C}$) |
|----------|------------------------------|--------------------------|---|
| Al | 70 | 0.34 | 7.17 |
| FM-73 | 1.67 | 0.38 | 66 |

As the adhesive layer is very thin in this problem, and we are interested in stress concentration areas in the adhesive layer close the adhesive-adherend interface, denser mesh has been assigned to these areas, see in Figure 2. The element type selected is quadratic reduced integration plane strain element (CPE8R).

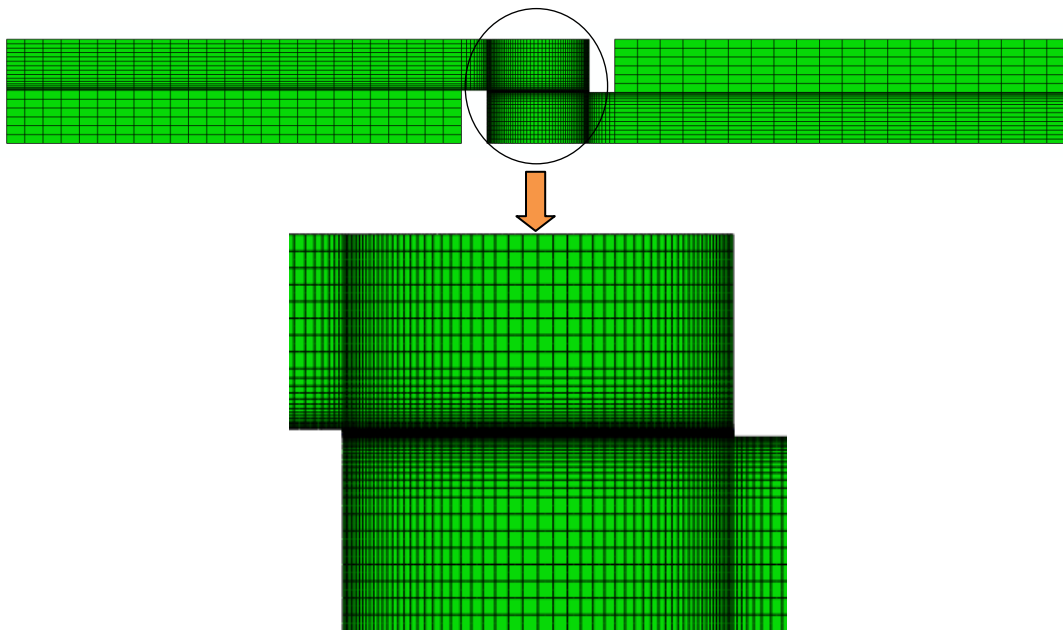


Figure 2: An example of finite element mesh for the model joint.

2.2.1. *Stress distribution along overlap length*

From equation (5), we notice that the parameters τ_i in the Prony series for FM-73 are relatively small, which means the material will relax and come to a steady state very quickly. Therefore, the stress states at two time steps, $t = 2s$, and $t = 50s$ are used. Figure 3 and Figure 4 show the comparison of shear stress and peel stress along the overlap length at $t = 2s$ and $t = 50s$. The location of the path along the overlap length in the viscoelastic adhesive selected is at 1/16 of the thickness from the upper adhesive-adherend interface where it is very close to the interface stress concentration area. Comparison of the shear stress results at $t = 2s$ and $t = 50s$ is shown in Figure 3. For both curves, the traction-free boundary conditions on the free ends lead to zero shear stress values on free ends, and therefore small shear stress values approaching zero can be observed at the integrating points adjacent to them. There is a sharp peak close to left free end and another smaller peak close to the right free end due to the geometric singularity of the corner and different material properties of the adjacent edge. Comparing the results for different time steps, it is shown that the shear stress result for $t = 2s$ has higher value than those at $t = 50s$ especially on the left and right peaks of the curves. This is because of the decrease of relaxation modulus with time, which results in a lower shear stress value for $t = 50s$ than that for $t = 2s$. In Figure 4, it can be seen that the peel stress values do not have much difference for $t = 2s$ and $t = 50s$, except that at the left free end the peak peel stress value for $t = 2s$ is higher than that of $t = 50s$. The above results are in reasonably good agreement with those presented in Roy and Reddy's work [21] which uses nonlinear viscoelastic finite element analysis.

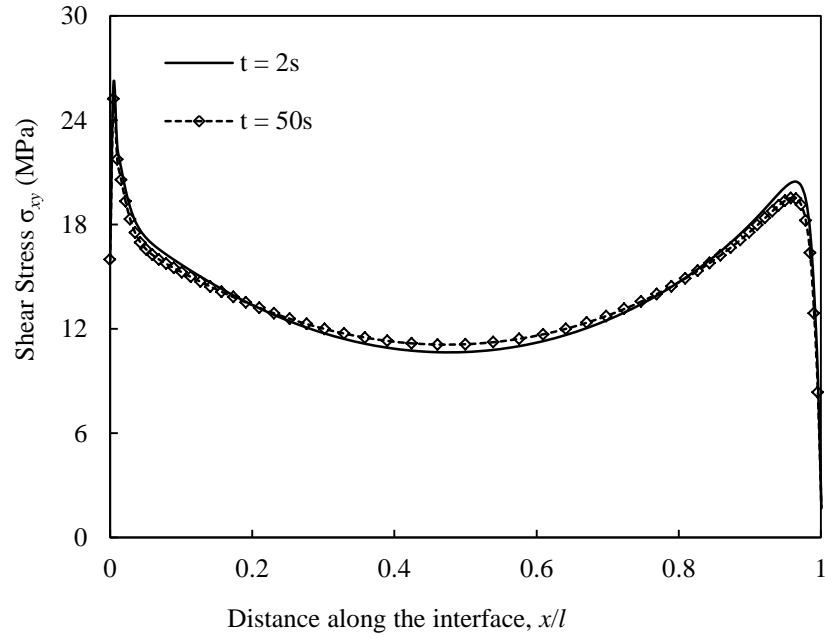


Figure 3: Shear stress distributions along overlap length (l) at time $t = 2s$ and $t = 50s$.

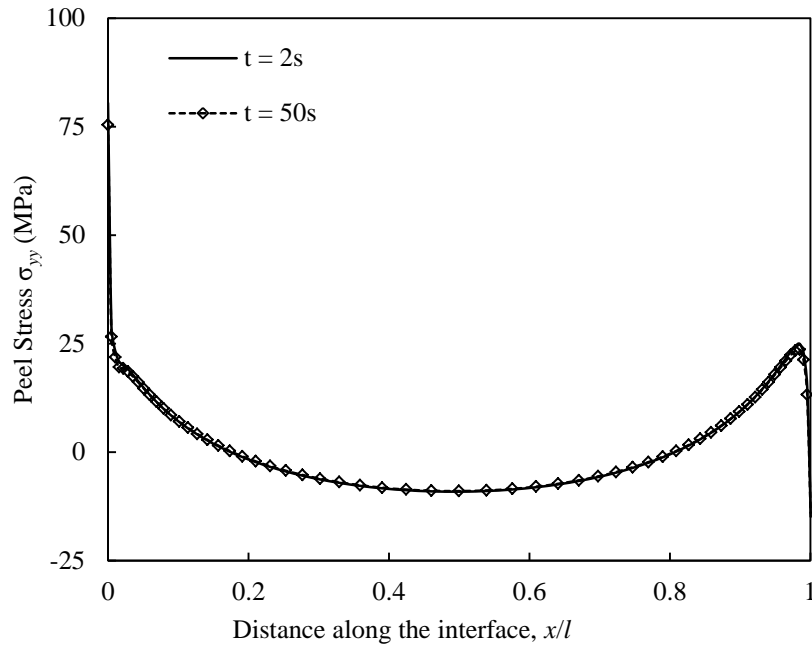


Figure 4: Peel stress distributions along overlap length (l) at time $t = 2s$ and $t = 50s$.

2.2.2. Effect of thermal expansion

The effect of thermal expansion on the viscoelastic adhesively bonded joint has also been studied. Comparisons of the shear and peel stress distributions for temperatures equal to 20, 220, and 420°C (or $\Delta T = 0, 100, 200, 400^\circ\text{C}$), at $t = 50\text{s}$ in the adhesive layer under constant stress $q_x = 13.6\text{ MPa}$ at 1/16 of the thickness from the upper adhesive-adherend interface are shown in Figure 5 and Figure 6. For shear stresses, first thing to notice is that when $\Delta T = 100^\circ\text{C}$, the resultant thermal stress induced by the difference in CTEs of the adhesive and adherend materials balances the uneven distribution of shear stress along overlap length. Then when temperature continuously rises ($\Delta T = 200, 400^\circ\text{C}$), compared to $\Delta T = 0^\circ\text{C}$, it reverses the shear stress distribution regarding the normal central line of the overlap length. Also for $\Delta T = 100, 200, 400^\circ\text{C}$, as ΔT increases, the absolute values of shear stress close to the two free ends and the right peak increase while the absolute value of the left inflection point decreases, see in Figure 5. For peel stress, the values at the two free ends do not change much as ΔT increases, but the values at the two inflection points increase as ΔT increases, shown in Figure 6(a). More detailed views of the areas close to the left and right free ends are shown in Figure 6(b) and 6(c), respectively. Comparing to shear stress, peel stresses along the overlap length do not experience a direction change during thermal expansion process, and they have smaller percentage change compared to shear stresses.

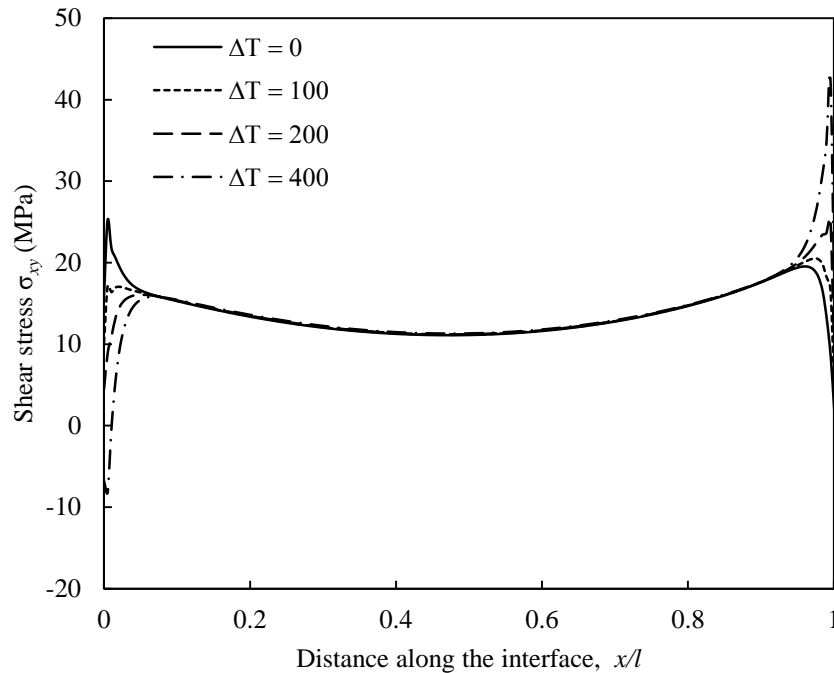
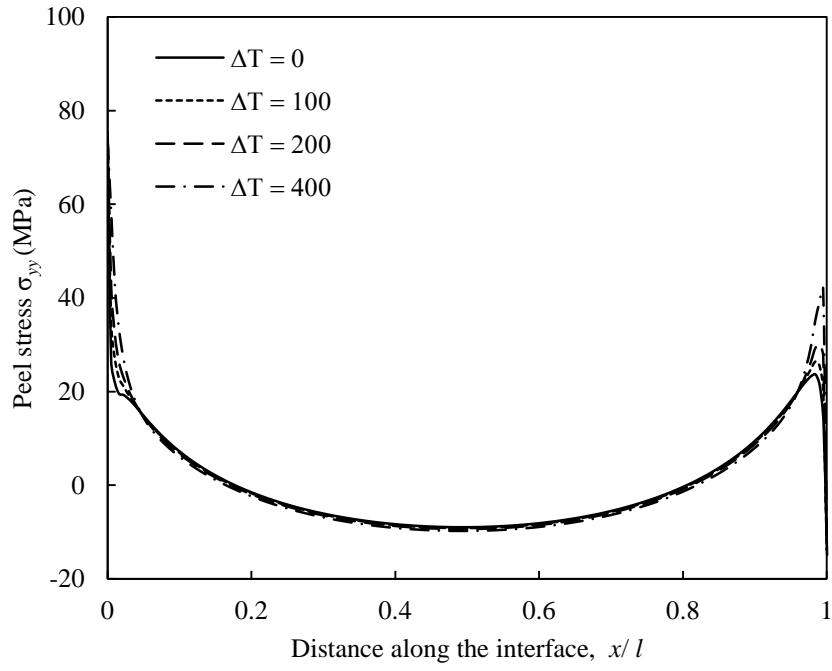
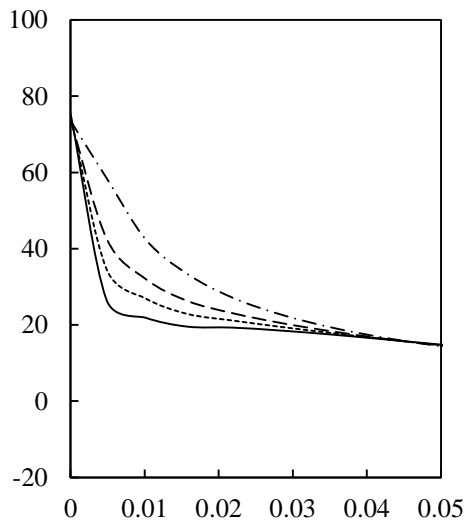


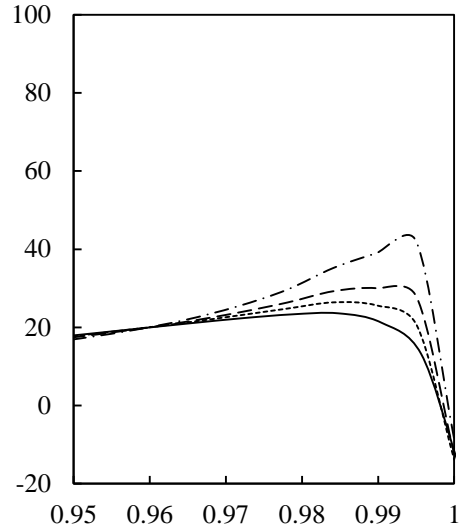
Figure 5: Shear stress distributions along overlap length (l) with various ΔT at $t = 50\text{s}$.



(a)



(b)



(c)

Figure 6: Peel stress distributions along overlap length (l) with various ΔT at $t = 50$ s. (a) Along total overlap length, (b) Local view of area close to left end, (c) Local view of area close to right end.

3. Damage analysis of viscoelastic adhesively bonded joints

3.1. Constitutive relation of cohesive element

3.1.1. Linear elastic traction-separation law

In cases where the critical energy release rate is the only given parameter, the cohesive zone modeling in finite element analysis is troublesome because it depends on critical energy release rate, maximum traction and the type of the traction-separation law. It is more straightforward to define the constitutive response by traction-separation law and model the top and bottom interfaces between adherends and adhesive using cohesive elements. The traction-separation law is typically characterized by peak strength and fracture energy. In the present study, a linear elastic traction-separation law is assumed prior to damage. Figure 7 shows a typical traction-separation response in one direction, where t_{\max} can be the maximum values of the three components t_n, t_s and t_t of nominal stress vector \mathbf{t} in 3D. t_n is the component of \mathbf{t} normal to the likely debonding surface, while t_s and t_t are the two shear components on the likely debonding surface. δ_0 is the critical displacement upon damage initiation, and the K is the penalty stiffness that relates the nominal stress to the displacement.

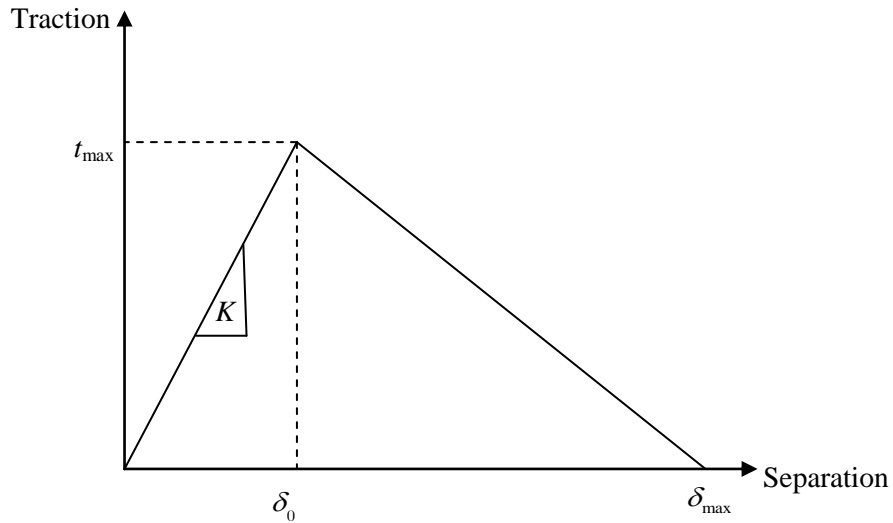


Figure 7: Traction-separation constitutive response.

3.1.2. Damage initiation and evolution

Damage initiation refers to the beginning of degradation of the material stiffness. The damage initiates when the stresses satisfy the quadratic nominal stress criterion which is given in equation (6)

$$\left(\frac{t_n}{N_{max}}\right)^2 + \left(\frac{t_s}{S_{max}}\right)^2 + \left(\frac{t_t}{T_{max}}\right)^2 = 1 \quad (6)$$

where N_{max} , S_{max} , and T_{max} represent the maximum values of the nominal stress components t_n , t_s , and t_t , respectively.

Damage evolution describes the rate of degradation of the material stiffness after the damage initiation. It can be specified either in terms of fracture energy or in terms of the equivalent plastic displacement. The fracture energy is defined as a function of mixed-mode which uses the power law expression as given in equation (7). G_{IC} , G_{IIC} , G_{IIIC} are the critical strain energy release rates for Mode I, II and III, respectively.

$$\left(\frac{G_I}{G_{IC}}\right)^\alpha + \left(\frac{G_{II}}{G_{IIC}}\right)^\alpha + \left(\frac{G_{III}}{G_{IIIC}}\right)^\alpha = 1 \quad (7)$$

The critical strain energy release rate G_{IC} measured by the critical energy release rate in a DCB test is the most important parameter that defines the cohesive traction-separation behavior. Besides, the value of separation at the final failure and the shape of the softening portion of the traction-separation curve are other parameters to be determined. In this work, once the damage is initiated by the quadratic nominal stress criterion, the damage evolution follows according to the given damage evolution law in equation (7). In the following numerical example, finite element analysis of a 2D plain strain problem has been conducted. The values of G_{IC} and G_{IIC} are from [37], which are measured by the critical energy release rate in DCB test and edge notch flexure (ENF) test, respectively. Separation force and delamination length for FM-73 are also provided in the same reference, which are used to determine the maximum normal and tangential traction strengths of the material.

3.2. Numerical example

In this section, a single lap shear joint is taken as an example for finite element damage analysis of viscoelastic adhesively bonded joints. The geometry and boundary conditions are taken from the model joint in [22], see in Figure 8. The adhesive thickness is 0.32 mm, very thin compared to

the dimensions of the adherends. Fixed boundary condition is applied on the left end of the bonded joint system. On the right end, vertical displacement u_y is zero at top and bottom of the adherend. Uniform stress is applied on the right end with the rates of 15 MPa/s and 7.5 MPa/s, respectively. Steel is used as adherend here with $E = 200$ GPa and $\nu = 0.33$, while FM-73 is used as adhesive material.

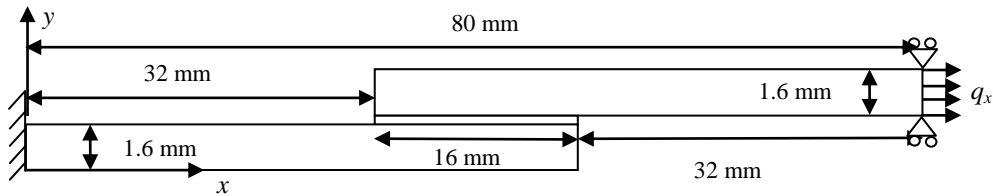


Figure 8: Geometry and boundary conditions for the model joint.

To apply traction-separation law, two layers of interface elements, with 112 elements on each, are added at the top and bottom interfaces along A1-A2 and B1-B2 lines in the single lap joint, as shown in Figure 9. These elements are four-node cohesive elements (COH2D4) with zero thickness, which are used to model interfacial debonding using traction-separation law in cohesive zone framework. In other words, it is the cohesive elements that include all the information regarding traction-separation behavior, damage initiation and evolution in this finite element model. For the rest of the model, four-node quadrilateral full integration plane strain elements (CPE4) are used. It is observed that if the value of the maximum stress is set higher than the maximum allowable stress in adjacent materials connected to the cohesive element, then the problem cannot be solved. Also, if the effective cohesive stiffness is set higher than the elastic modulus of the adjacent material, instead of the bond failure, the bulk material fails first.

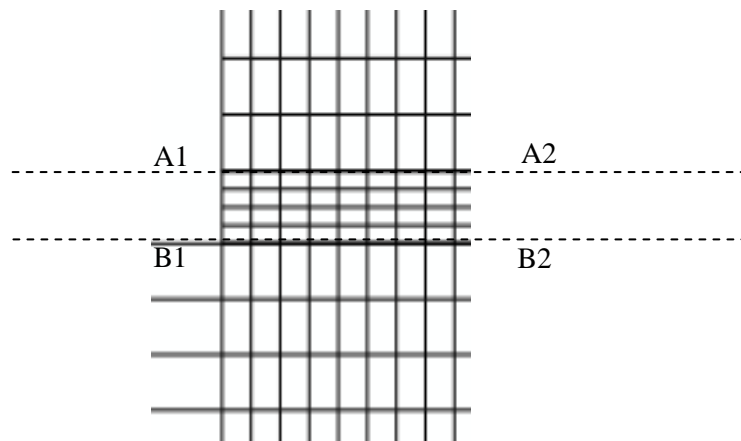


Figure 9: Cohesive elements along interfaces.

3.2.1. Joint stiffness

In the single lap shear test, the joint stiffness is represented by the relationship between applied load at the end of the bonded joint system and corresponding displacement at the end. Joint stiffness reflects the general load carrying ability of the bonded joint system, although it does not give detailed information about adhesive-adherend interfaces and local stress concentration areas. Figure 10 shows the curves of the stress applied versus horizontal displacement on the right end of the bonded joint system when the loading rate is 7.5 MPa/s for adhesive with both elastic and viscoelastic material properties. We can see that once the cracks at the adhesive-adherend interfaces initiate from the ends, they start to propagate and the bonded joint system has lost the capability to carry more loads in both cases, which shown in Figure 10 is that q_x stops growing as the horizontal displacement increases. When one of cracks propagates through the whole overlap length, the bonded joint system will totally fail and q_x will drop to zero. However in the real experiments, the propagation of the crack usually occurs so fast that the curves obtained will not have the plateau parts as those in Figure 10. This means the bonded joint system will suddenly reach a complete failure and q_x becomes zero. Also, it can be seen that the elastic case fails at a lower q_x than the viscoelastic case. This is because as the relaxation modulus of viscoelastic adhesive decreases with time, elastic adhesive with Young's modulus equals to $E(0)$ will experience higher stress level in local stress concentration area and fail first. Therefore, the bonded joint system with elastic adhesive will not be able to carry more loads earlier and reach a smaller peak value of q_x than viscoelastic adhesive. Here we can conclude that when the relaxation modulus of viscoelastic adhesive has terms with bigger values of g_i and τ_i (in other words, $E(t)$ will eventually have a lower value and take longer time to relax), the joint stiffness of the system will be more enhanced.

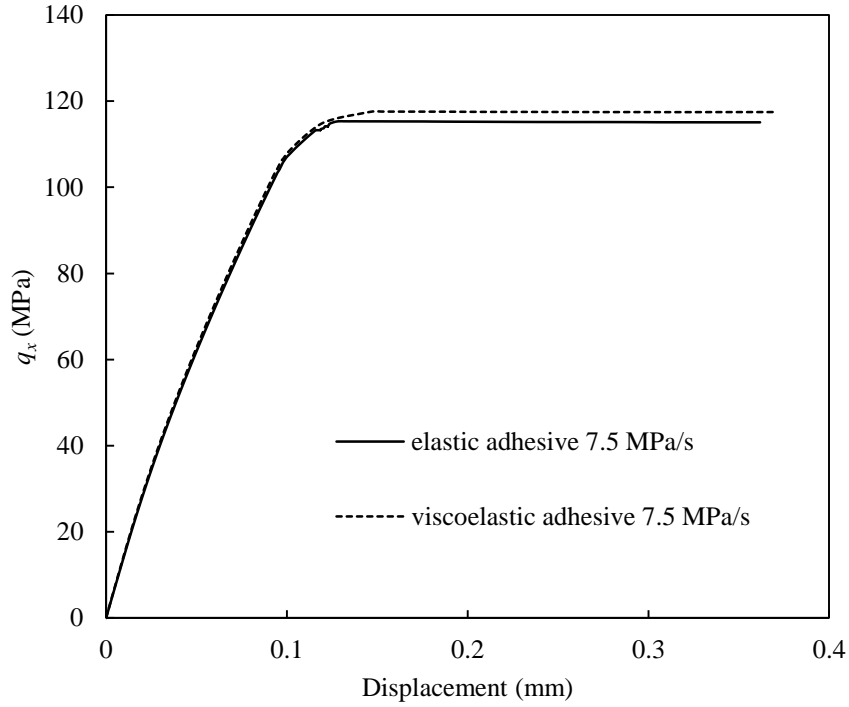


Figure 10: Stress applied vs. horizontal displacement at right end of the model joint.

3.2.2. Damage of cohesive elements

In the framework of continuum damage mechanics, damage is incorporated into global constitutive equations by introducing a scalar stiffness degradation value d , that accounts for the gradual decrease in elastic stiffness with accumulating damage in the material. The definition of d is given in equation (8), in which E and \bar{E} are the damaged Young's modulus and effective (undamaged) Young's modulus of the material, respectively.

$$E = (1 - d)\bar{E} \quad (8)$$

Figure 11 presents the scalar stiffness degradation value d of a cohesive element at the top interface on the right free end as a function of time for two loading rates 15 MPa/s and 7.5 MPa/s. The crack initiates when the maximum stiffness degradation is reached, which is taken as 0.99. In other words, element fails upon d reaching the maximum value of 0.99. It is shown in Figure 11 that the stiffness degradation of the selected element for two loading rates 15 MPa/s and 7.5 MPa/s suddenly starts around 0.6s and 0.1s respectively, and then grows very quickly until reaching the maximum value. The corresponding crack initiation time for the two loading rates are around 9s and 18s, respectively. The cohesive element under higher loading rate reaches the damage initiation and evolution criterion faster. The plots of cumulative crack length as a function of time at the top interface for loading rates of 15 MPa/s and 7.5 MPa/s are plotted in

Figure 12. Again, as expected, higher loading rate accelerates the crack initiation and propagation. Since the same linear elastic traction-separation law, damage initiation and evolution criteria are used in cohesive elements throughout all the simulations, the curves of scalar stiffness degradation versus applied load and cumulative crack length versus applied load for the two loading rates will simply fall on top of each other and therefore are not shown here.

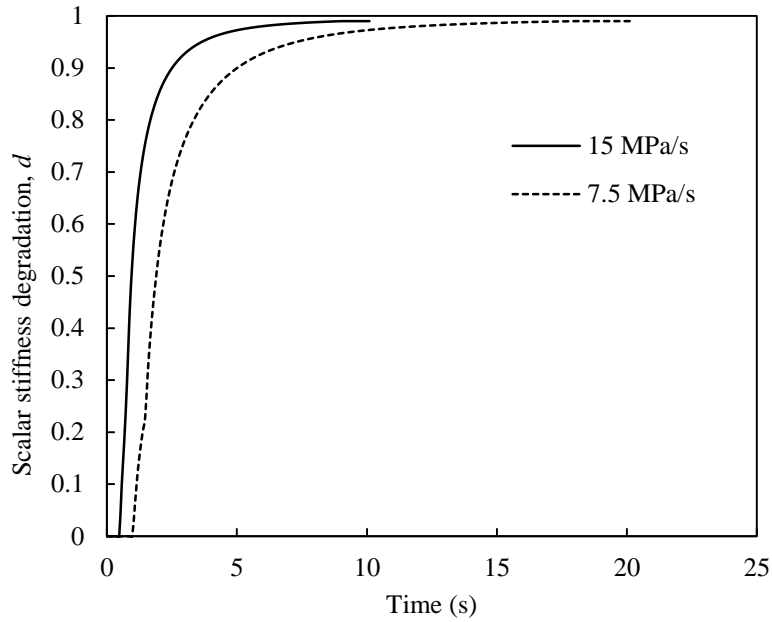


Figure 11: Scalar stiffness degradation value d vs. time for loading rates of 15 MPa/s and 7.5 MPa/s.

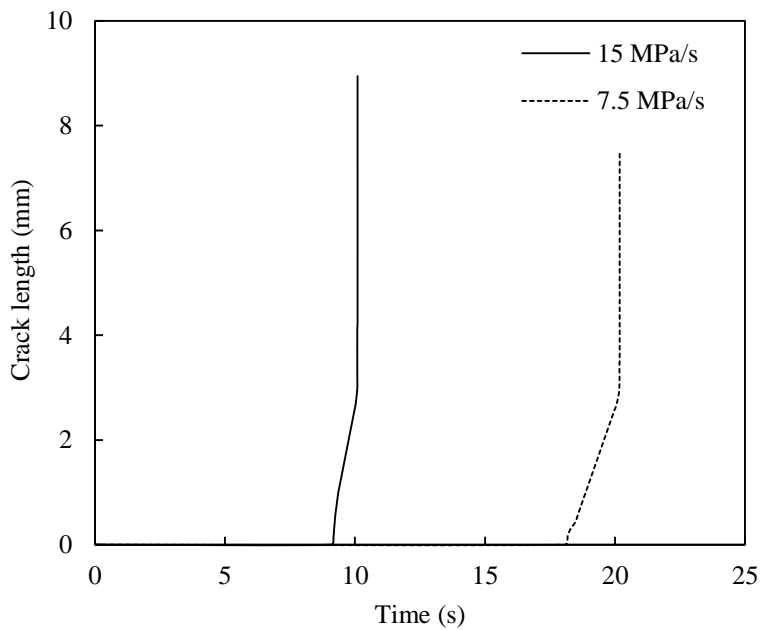


Figure 12: Cumulative crack length vs. time for loading rates of 15 MPa/s and 7.5 MPa/s.

In order to simulate the debonded interfaces, the failed elements are removed from the configuration, see in Figure 13. It is shown that the crack length of the top interface is much longer than that of bottom interface. The reason is due to the asymmetrical distributions of shear stress and peel stress along the overlap length. In the present case, elements close to right free end of the adhesive experience higher stress level than those close to left free end, which results in uneven crack length of top and bottom interfaces.

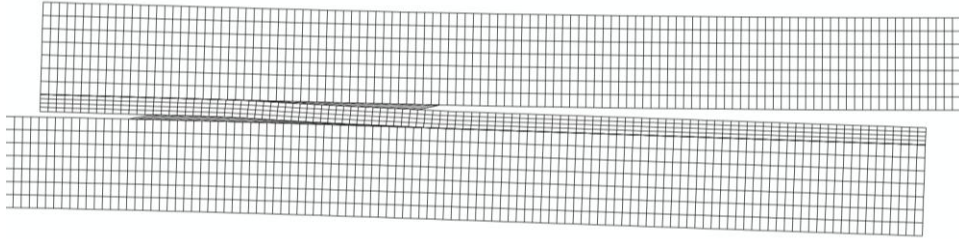


Figure 13: Damaged configuration of the single lap joint obtained from finite element model.

3.2.3. *Effects of interface damage on adhesive layer*

The effects of damage of cohesive elements at interfaces on stress distributions in adhesive layer have been investigated in this section. First, attention has been drawn to the change in stress distribution of plain strain elements within the adhesive along overlap length at different times. The loading rate used here is 7.5 MPa/s. Figure 14 shows the shear stress curves along overlap length within viscoelastic adhesive 0.08 mm (1/4 of adhesive thickness) from the top interface for times 2.07s, 5.07s, 10.07s and 15.07, respectively. Significant change in shear stress distribution along overlap length can be observed. As time increases, shear stress increases quite rapidly in general. Moreover, the peaks shift from the areas close to the free ends toward the middle of the overlap length. The reason for this is the increase in stiffness degradation of the cohesive elements which are close to the free ends on the interfaces, as shown in Figure 11. At the beginning, the cohesive elements close to the two free ends start to degrade first because they experience high stress level. Then, the stiffness degradation reduces the shear stress level in those areas and pushes the peaks toward the middle of overlap length where the material stiffness is relatively high. The change in peel stress along overlap length at different times is even more complex than that of shear stress, see in Figure 15. At time equals to 2.07s and 5.07s, the trend of peel stress change is similar to that of shear stress: value increases, peaks shift toward middle of overlap length. However, as loading continuously increases, due to the bending moment in the bonded joint system, the peel stress in the middle part changes from tension to compression and

forms a new peak in negative direction, which becomes the largest peak value (in absolute value) along overlap length.

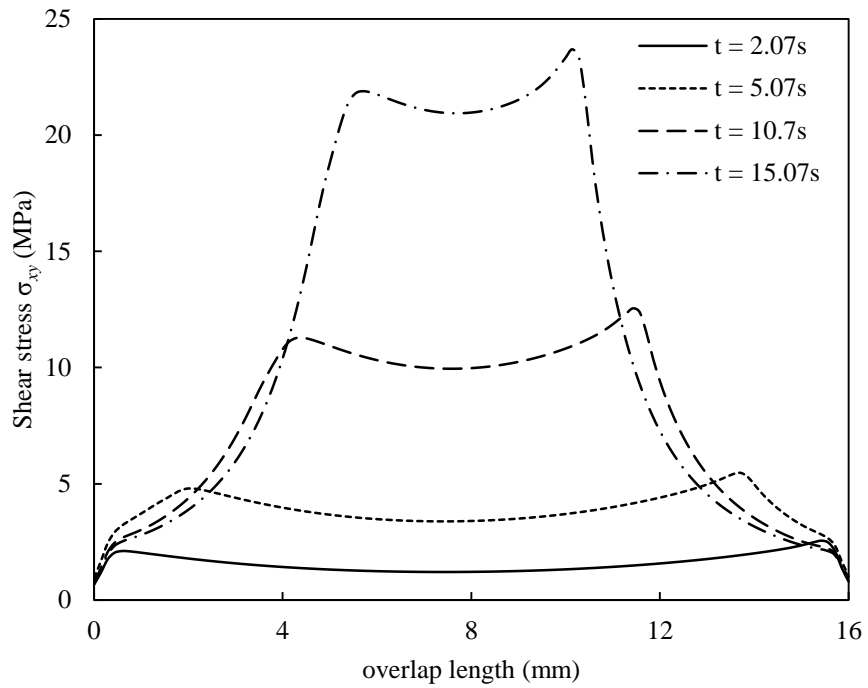


Figure 14: Shear stress distributions along overlap length at different times.

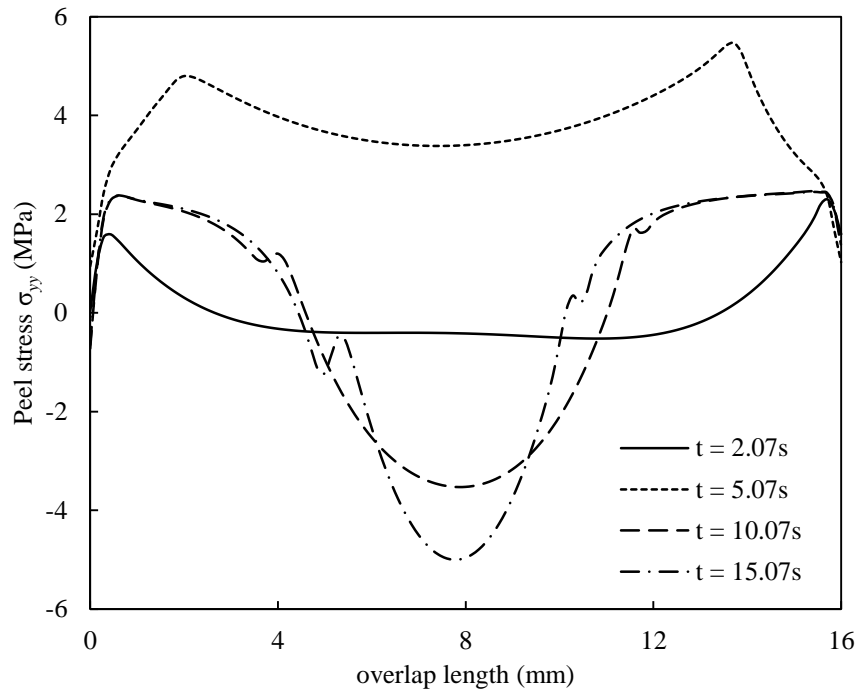


Figure 15: Peel stress distributions along overlap length at different times.

Second, the time histories of shear stress and peel stress for a plain strain element within the adhesive at the top interface crack tip have been studied. At the same loading rate 7.5 MPa/s, the results for elastic adhesive and viscoelastic adhesive are compared to show the influence of viscoelastic behavior on the adhesive layer in this damage process. In Figure 16, both elastic and viscoelastic adhesive shear stress curves have three stages: first, an initial sharp growth stage; second, “hardening-softening-plateau” stage when stiffness degradation in the adjacent cohesive element initiates and increases; and the last stage, debonding, when the adjacent cohesive element totally fails and loses load carrying ability. Also it can be noticed that there are jumps in stress at the last stage which indicates the instability of the crack propagation. On the other hand, we can see that the shear stress of elastic case reaches a higher value than that of viscoelastic case, which is because for positive strain rate the stress in elastic case grows faster than that in viscoelastic case. The peel stress curves also have three stages. But different than shear stress, peel stress exhibits only “softening-plateau” like behavior in the second stage and for the same reason the peel stress for elastic case decreases faster than the viscoelastic case with time, see in Figure 17. Therefore, the peel stress for elastic case has a smaller value than that of viscoelastic case in the “softening-plateau” stage. Furthermore, it is shown that viscoelasticity has more influence on shear stress than peel stress for time history in the present single lap joint model.

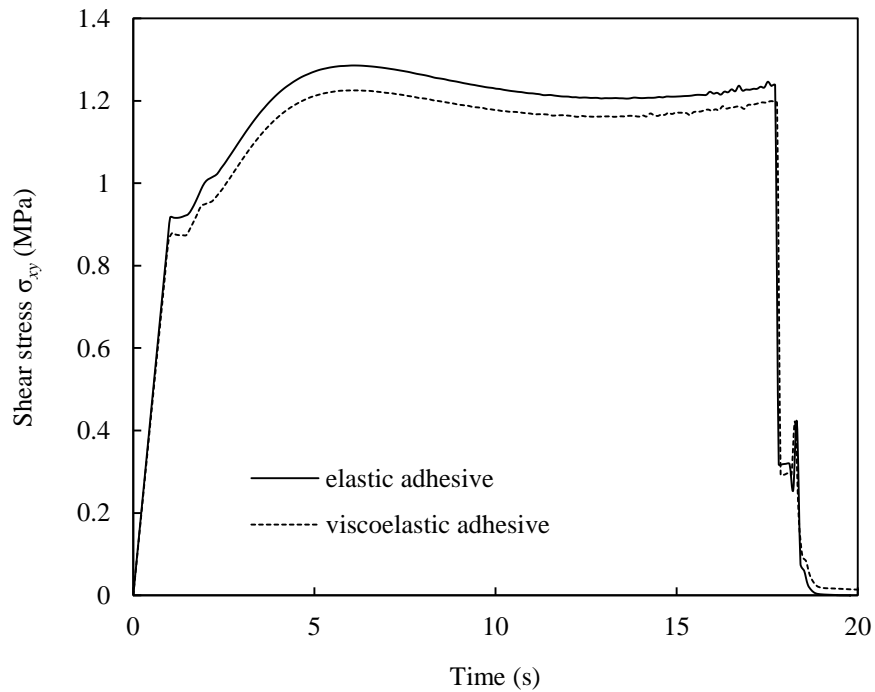


Figure 16: Shear stress vs. time.

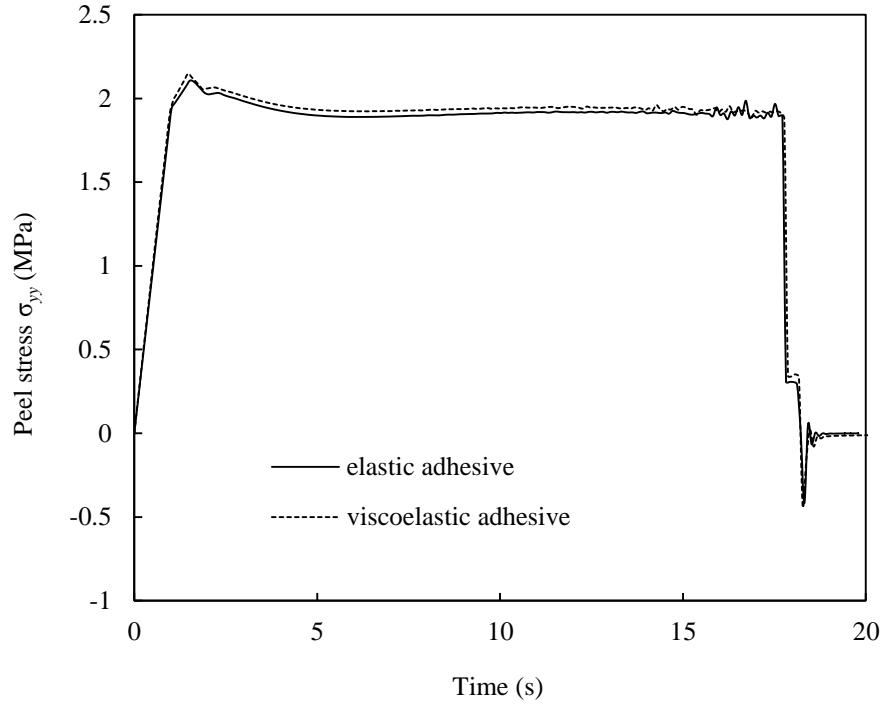


Figure 17: Peel stress vs. time.

4. Summary and Conclusions

In this study, linear viscoelastic behavior and interface failure in adhesively bonded joints have been studied. FM-73 with linear viscoelastic material properties has been used as adhesive, while the materials used for adherend are aluminum and steel. Finite element analysis considering geometric nonlinearity as well as thermal expansion has been carried out. The benchmark problem from [21] is used as a validation example, and the results of the present model are found in good agreement with those in [21]. Then thermal expansion is taken into consideration, and it is shown to be a very important factor that influences the stress distribution in the high stress concentration areas of adhesive. In the model joint, as temperature increases, the difference in CTEs of the adhesive and adherend materials changes the shear stress direction close to the interface area. For peel stress, peak value increases as temperature rises. Also, it is noticed that the shear stress is affected more than the peel stress by thermal expansion. Furthermore, to study the damage behavior of the interfaces between the adhesive and the adherend, the cohesive zone model in ABAQUS [36] with linear elastic traction-separation law is applied. The bond failure analysis for both elastic adhesive and viscoelastic adhesive at certain loading rates has been carried out. By comparing to elastic adhesive, it is found that viscoelastic adhesive can enhance the stiffness of the bonded joint system. From the results of the cohesive zone model at adhesive-

adherend interfaces, it is observed that the higher loading rate can accelerate the crack initiation and propagation at the adhesive-adherend interfaces. Finally, the influences of interface damage on the stress in adhesive layer are discussed. First, shear and peel stress curves along overlap length at different times are plotted. Due to the stiffness degradation in the cohesive elements, the stress distribution along overlap length changed significantly over time: peaks of the stress curves transfer from close to the free ends toward the middle of the overlap length. Second, time histories of shear stress and peel stress of a plain strain element in adhesive at the crack tip have been studied. Quick growth in stress value and debonding from the interface of the plain strain element can be observed for both shear stress and peel stress at the beginning and the end of the time history, respectively. In between, shear stress shows a “hardening-softening-plateau” like behavior, whereas peel stress exhibits a “softening-plateau” character. Also, it is shown that the shear stress is more affected than the peel stress by the viscoelastic material properties of the adhesive.

Acknowledgements

The research reported here was carried out under MURI09 grant (Award No. FA-9550-09-1-0686) from the Air Force Office of Scientific Research. The authors acknowledge many discussions during the course of this research with Dr. Ozden Ochoa.

References

- 1 R. D. Adams and N. A. Peppiatt, *J. Strain Analysis Eng. Design* **9**, 185 (1974).
- 2 I. U. Ojalvo and H.L. Eidinoff, *AIAA J.* **16**, 204 (1978).
- 3 M. Goland and E. Reissner, *J. Appl. Mech* **11**, A17 (1944).
- 4 F. Delale, F. Erdogan and M. N. Aydinoglu, *J. Composite Mater.* **15**, 249 (1981).
- 5 B. Zhao and Z.-H. Lu, *Mech. Adv. Mater. Struct.* **16**, 130 (2009).
- 6 B. Zhao, Z.-H. Lu and Y.-N. Lu, *Intl. J. Adhesion Adhesives* **31**, 434 (2011).
- 7 J. N. Reddy and S. Roy, *Intl. J. Non-Linear Mech.* **23**, 97 (1988).
- 8 W. C. Carpenter, *Intl. J. Numer. Methods Eng* **15**, 1659 (1980).
- 9 P. A. Cooper and J.W.Sawyer, NASA technical paper 1507, PLASTECH, Dover, NJ (1979).
- 10 G. Li, P. Lee-Sullivan and R.W. Thring, *Composite Structures* **46**, 395 (1999).
- 11 A. G. Magalhães, M. F. S. F. de Moura and J. P. M. Gonçalves, *Intl. J. Adhesion Adhesives* **25**, 313 (2005).
- 12 C. Yang, H. Huang, J. S. Tomblin and W. Sun, *J. Composite Mater.* **38**, 293 (2004).

- 13 S. Yadagiri, C. P. Reddy and T. S. Reddy, *Computers and Structures* **27**, 445 (1987).
- 14 W. C. Carpenter, *Computers and Structures* **36**, 1141 (1990).
- 15 M. Henriksen, *Computers and Structures* **18**, 133 (1984).
- 16 R. A. Schapery, A&S Report No.69-2, Purdue University, W. Lafayette, IN (1969).
- 17 D. Peretz and Y. Weitsman, *J. Rheology* **27**, 97 (1983).
- 18 W. G. Knauss and I. J. Emri, *Computers and Structures* **13**, 123 (1981).
- 19 E. B. Becker et al., AFWAL-TR-84-4057, General Dynamics, Fort Worth Division, TX (1984).
- 20 S. Roy and J. N. Reddy, *Computers and Structures* **29**, 1011 (1988).
- 21 S. Roy and J. N. Reddy, *Tire Sci. Technol.* **16**, 146 (1988).
- 22 S. Roy and J. N. Reddy, *Intl. J. Numer. Meth. Eng.* **26**, 2531 (1988).
- 23 B. G. Schaffer and D. F. Adams, *J. Appl. Mech.* **48**, 859 (1981).
- 24 W. G. Knauss, *The Deformation in Fracture of High Polymers*, New York: Plenum, 501 (1973).
- 25 R. A. Schapery, *Intl. J. Fracture* **11**, 369 (1975).
- 26 R. A. Schapery, *Intl. J. Fracture* **11**, 549 (1975).
- 27 R. A. Schapery, *Intl. J. Fracture* **11**, 141 (1975).
- 28 W. G. Knauss, *J. Eng. Mater. Technol., Trans. ASME* **115**, 262 (1993).
- 29 W. G. Knauss and G. U. Losi, *J. Appl. Mech., Trans. ASME* **60**, 793 (1993).
- 30 D. H. Allen and C. R. Searcy, *Intl. J. Fracture* **107**, 159 (2001).
- 31 B. Chen and D. A. Dillard, *Intl. J. Solids Structures* **38**, 6907 (2001).
- 32 F. Dubois, C. Chazal and C. Petit, *Mech. Time-Dependent Materials* **2**, 269 (1998).
- 33 P. Rahul Kumar, A. Jagota, S. J. Bennison and S. Saigal, *Intl. J. Solids Structures* **37**, 1873 (2000).
- 34 A. Muliana and K. A. Khan, *Computational Mater. Sci.* **41**, 576 (2008).
- 35 J. N. Reddy, *An Introduction to Continuum Mechanics*, Cambridge University Press, New York (2008).
- 36 ABAQUS, *USER MANUAL* **6.8.3**.
- 37 O. Ishai, H. Rosenthal and E. D. N. Sela, *Composites* **19**, 49 (1988).